Atmos. Meas. Tech., 6, 2907–2924, 2013
www.atmos-meas-tech.net/6/2907/2013/
doi:10.5194/amt-6-2907-2013

Atmospheric Measurement Techniques
Open Access

Comparison of tropospheric NO_2 vertical columns in an urban environment using satellite, multi-axis differential optical absorption spectroscopy, and in situ measurements

D. Mendolia[1], **R. J. C. D'Souza**[1], **G. J. Evans**[1], **and J. Brook**[2]

[1]Southern Ontario Centre for Atmospheric Aerosol Research (SOCAAR), University of Toronto, 200 College St., Toronto, M5S 3E5, Ontario, Canada
[2]Environment Canada, 4905 Dufferin St., Toronto, M3H 5T4, Ontario, Canada

Correspondence to: G. Evans (greg.evans@utoronto.ca)

Received: 3 December 2012 – Published in Atmos. Meas. Tech. Discuss.: 25 January 2013
Revised: 4 September 2013 – Accepted: 5 September 2013 – Published: 31 October 2013

Abstract. Tropospheric NO_2 vertical column densities have been retrieved and compared for the first time in Toronto, Canada, using three methods of differing spatial scales. Remotely sensed NO_2 vertical column densities, retrieved from multi-axis differential optical absorption spectroscopy and satellite remote sensing, were evaluated by comparison with in situ vertical column densities estimated using a pair of chemiluminescence monitors situated 0.01 and 0.5 km a.g.l. (above ground level). The chemiluminescence measurements were corrected for the influence of NO_z, which reduced the NO_2 concentrations at 0.01 and 0.5 km by an average of 8 ± 1 % and 12 ± 1 %, respectively. The average absolute decrease in the chemiluminescence NO_2 measurement as a result of this correction was less than 1 ppb. The monthly averaged ratio of the NO_2 concentration at 0.5 to 0.01 km varied seasonally, and exhibited a negative linear dependence on the monthly average temperature, with Pearson's $R = 0.83$. During the coldest month, February, this ratio was 0.52 ± 0.04, while during the warmest month, July, this ratio was 0.34 ± 0.04, illustrating that NO_2 is not well mixed within 0.5 km above ground level. Good correlation was observed between the remotely sensed and in situ NO_2 vertical column densities (Pearson's R value ranging from 0.72 to 0.81), but the in situ vertical column densities were 52 to 58 % greater than the remotely sensed columns. These results indicate that NO_2 horizontal heterogeneity strongly impacted the magnitude of the remotely sensed columns. The in situ columns reflected an urban environment with major traffic sources, while the remotely sensed NO_2 vertical column densities were representative of the region, which included spatial heterogeneity introduced by residential neighbourhoods and Lake Ontario. Despite the difference in absolute values, the reasonable correlation between the vertical column densities determined by three distinct methods increased confidence in the validity of the values provided by each measurement technique.

1 Introduction

In Canada, nitrogen oxides ($NO_x = NO + NO_2$) are classified as criteria air contaminants due to their adverse effects on human health and the environment (Environment Canada, 2013). Anthropogenic production of NO_x is largely attributed to fossil fuel combustion, with the transportation sector accounting for 68 % of NO_x emissions in Ontario during 2008 (MOE, 2011). Previous studies investigating the spatial distribution of NO_x have focused on near-road environments as a means to assess human exposure to traffic-related air pollution (TRAP), characterize TRAP dilution and chemical evolution, inform urban infrastructure planning and policy, and validate dispersion models (Villena et al., 2011; McAdam et al., 2011; Y. J. Wang et al., 2011; Clements et al., 2009; Beckerman et al., 2008). These studies suggest that variability in traffic volume and fleet characteristics, as well as local topography and meteorological conditions, impact the NO_x concentration (distance–decay) gradients observed amongst different near-road environments. Negative

health effects associated with exposure to NO_2 when used as a marker for TRAP include the exacerbation of asthma symptoms, the increased risk of developing cardiovascular and lung diseases, and increased mortality rates (Andersen et al., 2011; Valari et al., 2011; Pereira et al., 2010; Jerrett et al., 2009; Salam et al., 2008, and references therein; Nafstad et al., 2003). Therefore, an effective means of monitoring the spatio-temporal behaviour of NO_2 could do much to support the development of appropriate pollution mitigation strategies.

Satellite measurements of tropospheric NO_2 vertical column densities (VCDs) can provide long-term spatio-temporal trends on a global-to-regional scale. The Ozone Monitoring Instrument (OMI) was launched on board NASA's EOS-Aura satellite on 15 July 2004, and provides daily tropospheric NO_2 column measurements with a spatial resolution up to $13 \times 24\,km^2$ at nadir. OMI has a local ascending equatorial crossing time of 13:45 EST (Levelt et al., 2006). Previous studies have extended the utility of OMI tropospheric NO_2 column measurements to validate and improve chemical transport models (e.g. S. Wang et al., 2011; X. Wang et al., 2011; Hains et al., 2010; Huijnen et al., 2010), provide top-down emission estimates of NO_x and validate bottom-up emission inventories (Shaiganfar et al., 2011; Lamsal et al., 2010), quantify long-term trends in NO_x emissions over continental source regions (Boersma et al., 2008b), separate anthropogenic NO_2 emissions from biomass burning events (Mei et al., 2011), estimate the lifetime of tropospheric NO_x and account for observed seasonal patterns (Lamsal et al., 2010), infer NO_2 surface concentrations and associated long-term trends (Lee et al., 2011; Lamsal et al., 2008), and analyse the impact of precursor species on surface O_3 formation (Duncan et al., 2010). Although OMI tropospheric NO_2 columns have been applied to inform a variety of objectives, there is still a strong need for independent validation measurements (Vlemmix et al., 2010; Celarier et al., 2008; Irie et al., 2008), especially since previous validation studies have demonstrated that the relationship between OMI and field measurements varies from region to region (Hains et al., 2010).

Previous studies have assessed the relationship between ground-based and satellite tropospheric NO_2 VCDs, and have established that VCDs derived from localized-point measurements can directly capture near-source emissions of NO_2, while the large spatial footprint ($\geq 312\,km^2$) of satellite measurements makes it challenging to retrieve this information (Boersma et al., 2009; Ordóñez et al., 2006; Petritoli et al., 2004). These studies have relied on extrapolating ground-based NO_2 measurements to derive VCDs, either by assuming a well-mixed planetary boundary layer (PBL), or using a computationally intensive global chemical and transport model (CTM) with coarse resolution ($> 250\,km^2$) to derive a vertical NO_2 profile.

On a regional and short-term scale, Ontario's Air Quality Index informs the public about their potential to experience adverse health effects from outdoor air, relying on hourly average in situ measurements of pollutants such as NO_2, $PM_{2.5}$ and O_3 (MOE, 2010b). In downtown Toronto, NO_x monitoring stations situated at 0.01 and 0.5 km a.g.l. (43.663° N, 79.388° W and 43.642° N, 79.387° W) provided the opportunity to examine tropospheric vertical profiles of NO_2 in a near-road environment, and to demonstrate that NO_2 is not well mixed within 500 m a.g.l. These monitoring stations enabled the retrieval of a NO_2 vertical profile with a horizontal resolution of 2.3 km, which is advantageous in comparison to using a CTM, since few models can derive a NO_2 vertical profile with a horizontal resolution less than 5 km on a local scale. Furthermore, the use of a local-scale CTM requires a well-characterized emissions inventory (Bechle et al., 2013; Simpson et al., 2012), which currently does not exist for Toronto. Studies relying on a local-scale CTM have still used simplifying assumptions regarding the free-tropospheric quantity of NO_2, which has previously been assumed to be constant at 0.02 ppb above 2 km (Bechle et al., 2013).

Multi-axis differential optical absorption spectroscopy (MAX-DOAS) is a relatively new technique used to retrieve tropospheric NO_2 columns that is well suited for the validation of coincident OMI measurements (Halla et al., 2011; Vlemmix et al., 2010). MAX-DOAS employs intensity measurements of scattered sunlight at a series of elevation angles, relying on the narrowband absorbance structures of NO_2 within the UV–visible wavelength range, to obtain tropospheric vertical column densities (VCDs) of NO_2. Knowledge of average photon trajectories is essential for resolving NO_2 VCDs from MAX-DOAS spectra, but is an involved task, having previously been accomplished with radiative transfer modelling or trigonometric approximations. MAX-DOAS draws upon the advantages of both localized-point and satellite-based measurements, offering average pollutant concentrations covering a horizontal scale which has been reported to vary from 3 to 11 km ($\lambda = 357$ nm, aerosol extinction coefficient within 1 km a.g.l. varied from 1.02 to $0.05\,km^{-1}$) with a time resolution on the scale of a few minutes (Irie et al., 2011).

Previous studies have investigated the relationship between OMI and MAX-DOAS tropospheric NO_2 VCDs (Shaiganfar et al., 2011; Halla et al., 2011; Wagner et al., 2010; Vlemmix et al., 2010; Kramer et al., 2008; Brinksma et al., 2008; Celarier et al., 2008; Irie et al., 2008), and have demonstrated that a fair agreement was generally observed. Differences amongst the retrieved tropospheric NO_2 VCDs have been attributed to differences in the spatial resolution of ground and satellite remote sensing techniques, in addition to the vertical sensitivity of each instrument, and the NO_2 VCD retrieval algorithm employed.

The majority of studies suggest that OMI exhibits a positive bias over rural (unpolluted) MAX-DOAS measurement sites, and a negative bias over urban (polluted) MAX-DOAS measurement sites (Shaiganfar et al., 2011; Halla et al., 2011;

Table 1. Location of in situ monitoring sites and pollutants of interest.

Monitoring site		Location	Measurement height (m a.g.l.)	Monitored pollutants of interest	Vehicle counts (10^3 vehicles, 24 h average)*
A.	DT	Bay St./ Wellesley St. W (43.663° N, 79.388° W)	10	NO, NO_2, and O_3	17.4
B.	CN	301 Front St. W (43.642° N, 79.387° W)	445	NO, NO_2, and O_3	97.3

* 24 h average weekday vehicle counts include east and west-bound traffic (Toronto Transportation Services, 2010). DT refers to the Ontario Ministry of the Environment (MOE) Air Quality Network's downtown Toronto Site. CN refers to the MOE's monitoring site situated at the CN Tower.

Kramer et al., 2008; Brinksma et al., 2008; Celarier et al., 2008), despite the use of different OMI products (standard versus DOMINO product and versions of these products), MAX-DOAS instrumentation, and NO_2 VCD retrieval algorithms. While the OMI pixel size is $\geq 312\,km^2$, the horizontal resolution of the MAX-DOAS instrument decreases rapidly with increasing aerosol load. Therefore, when MAX-DOAS measurements are conducted at a rural site, coincident OMI pixels may include areas with high NO_2 concentrations, and alternatively, when MAX-DOAS measurements are conducted at an urban site, coincident OMI pixels may include areas with lower NO_2 concentrations.

Previous studies have also investigated the use of stricter coincidence criteria when comparing satellite- and ground-based remote sensing techniques as a means to overcome the differences in spatial resolution of the measurements, and improve their agreement. These criteria have included averaging MAX-DOAS VCDs over several azimuths (Brinksma et al., 2008; Celarier et al., 2008), only including OMI measurements with a pixel centre within $0.1° \times 0.1°$ of the MAX-DOAS measurement site (Irie et al., 2008), and excluding MAX-DOAS measurements with a relative uncertainty $\geq 10\,\%$ (Vlemmix et al., 2010). These studies demonstrated that using stricter coincidence criteria improves the agreement between MAX-DOAS and OMI measurements.

This study examines the influence of NO_2 horizontal heterogeneity in an urban environment on VCDs determined by three methods of differing spatial scales. The goal of this study was to evaluate the response of remotely sensed NO_2 vertical column measurements in regions with spatially heterogeneous emissions of NO_2 examined using in situ-derived column data. Specifically, remotely sensed tropospheric NO_2 VCD measurements from OMI (DOMINO product, version 2.0) and MAX-DOAS were evaluated through comparison with in situ tropospheric NO_2 VCDs determined based on data collected in the downtown core of Toronto, Ontario during select periods in 2006–2010. Tropospheric NO_2 VCDs were derived using data from in situ (chemiluminescence) monitors situated near roadside at 0.01 and 0.5 km a.g.l. This is the first study that uses stationary in situ measurements of NO_2 collected at two elevations to derive tropospheric NO_2 columns in an urban environment for comparison with remotely sensed data.

MAX-DOAS NO_2 differential slant column densities (ΔSCDs) were converted to tropospheric vertical column densities (VCDs) using the geometric air mass factor (AMF) approximation (Hönninger et al., 2004) in conjunction with the single-scattering validation criteria discussed by Halla et al. (2011) and Brinksma et al. (2008). The impact of NO_2 horizontal heterogeneity on the remotely sensed VCDs was assessed by comparing MAX-DOAS and OMI tropospheric NO_2 VCDs to those derived in situ (and near road).

This paper is structured as follows: Sect. 2 describes the methodology employed, providing an overview of the downtown Toronto measurement site, along with a description of the in situ, MAX-DOAS, and OMI instruments, and the respective NO_2 VCD retrieval algorithms. Section 3 presents the in situ-derived NO_2 VCD's temporal trends, and the comparison between point-source and remotely sensed tropospheric NO_2 columns. Conclusions are derived based on the findings from Sect. 3, and presented in Sect. 4.

2 Methodology

2.1 Description of downtown Toronto measurement sites

In situ, MAX-DOAS, and satellite data were collected during the period of March 2006–March 2010. Hourly averaged in situ data were obtained from NO_x chemiluminescence (CL), and O_3 ultraviolet photometry monitors (Thermo 42i and 49i) situated at the Ontario Ministry of the Environment (MOE) Air Quality Network's downtown Toronto Site (DT), located 10 m above ground level (MOE, 2010a) and 2.9 km north of Lake Ontario. A second set of NO_x and O_3 monitors (Thermo 49C and 42C) situated at the CN Tower (CN) sampled ambient air at 445 m a.g.l. and 2.3 km SSE of DT (0.6 km N of Lake Ontario), as shown in Fig. 1. The MOE's monitoring sites are characterized in Table 1. O_3 data were used to correct NO_2 measurements for interference from

Table 2. Monitoring period and associated observation geometry for MAX-DOAS measurements. The horizontal distance from the MAX-DOAS instrument (at the azimuth angle surveyed) to Lake Ontario is provided in the "Mainland Toronto" column.

Campaign	Monitored period	Location	Measurement height (m a.g.l.)	Elevation angles of interest (°)	Azimuth angle (°)	Mainland Toronto (km)
A.	1, 3, 6–7 Mar 2006	Wallberg Building (43.659° N, 79.390° W)	15	10, 20, 90	225	3.45
B.	13, 16–17 Jun 2006	Centre Island (43.624° N, 79.365° W)	5	10, 20, 90	30	*
C.	18–19, 27 Jul; 5, 8 Aug 2006	McLennan Physics Building (43.660° N, 79.398° W)	65	10, 20, 90	90	10.6
D.	13–17 Aug 2009	McLennan Physics Building	65	10, 30, 90	165	2.52
E.	16–19 Mar 2010	Wallberg Building	15	10, 20, 30, 90	165	2.25

* Campaign B surveyed 1.70 km over Lake Ontario prior to reaching mainland Toronto.

Fig. 1. Location of DT and CN monitoring sites characterized in Table 1. Location of MAX-DOAS instrument during campaigns in Table 2: 1 = Wallberg Building, 2 = Centre Island, and 3 = McLennan Physics Building. The four points surrounding the MAX-DOAS and in situ measurement locations refer to the corners of a 13 km × 24 km OMI pixel with its area centred on DT.

NO_z, using the procedure reported by Boersma et al. (2009), which is discussed in Sect. 2.2. The in situ measurements of NO_2 provided the opportunity to observe the impact of diurnal traffic patterns and associated meteorology on the spatio-temporal distribution of NO_2 in an urban environment.

MAX-DOAS measurements were conducted at the University of Toronto's Wallberg and McLennan Physics buildings, as well as at Toronto's Centre Island, as summarized in Table 2. Azimuth angles were chosen based on the constraints of each monitoring site's topography to ensure buildings and trees did not obstruct the MAX-DOAS instrument's field of view. A map of the MAX-DOAS measurement sites is provided in Fig. 1.

An example OMI pixel from 27 May 2008 with its centre located at DT is also shown in Fig. 1. The in situ and MAX-DOAS measurement sites are well contained within this pixel. Approximately 60 % of the pixel area overlaps mainland Toronto, while the remaining 40 % is over Lake Ontario.

2.2 In situ NO_2 VCD retrieval

In situ-derived tropospheric NO_2 VCDs (NO_2 $VCD_{\text{in situ}}$) were calculated assuming that NO_2 exhibits an exponentially decaying vertical profile, as shown in Eq. (1) with $z = 12$ km. The value selected to describe the height of the troposphere (z) made no difference to the magnitude of the VCD as

$z \gg H_{NO_2}$. The characteristic height of NO_2 (H_{NO_2}) refers to the height at which the in situ NO_2 concentration at DT ($[NO_2]_{10m}$) decreases by a factor of e, assuming an exponential vertical profile. Mathematically, the same numeric value for the height could describe a fully mixed layer with a concentration equal to that at DT, or a combination of a fully mixed layer under an exponentially decaying layer. While the assumption of an exponentially decaying vertical profile was reasonable and was the best possible representation based on the available data, these data did not demonstrate that the profile was in fact exponential.

The characteristic height was derived using the in situ NO_2 concentration at DT ($[NO_2]_{10m}$) and at CN ($[NO_2]_{445m}$), as shown in Eq. (2), where $z = 435$ m. An increase in characteristic height indicates that NO_2 occupies a greater vertical fraction of the atmosphere. The NO_2 VCD in Eq. (1) is linearly dependent on H_{NO_2} in Eq. (2). Since $z \gg H_{NO_2}$, the term $[1 - \exp(-z/H_{NO_2})]$ in Eq. (1) essentially equals 1 at the tropopause, and as such Eq. (1) can be simplified to NO_2 $VCD_{in\ situ} = H_{NO_2}[NO_2]_{10m}$. Linear regression of NO_2 $VCD_{in\ situ}$ versus H_{NO_2} yields a slope of $[NO_2]_{10m}$.

$$NO_2\,VCD_{in\ situ} = H_{NO_2}\,[NO_2]_{10m}\left[1 - \exp\left(-z/H_{NO_2}\right)\right] \quad (1)$$

$$H_{NO_2} = 1/\left(\frac{1}{z}\ln\frac{[NO_2]_{10m}}{[NO_2]_{445m}}\right) \quad (2)$$

$$[NO_2]_z = [NO_2]_{10m}\left[\exp\left(-z/H_{NO_2}\right)\right] \quad (3)$$

The assumption of a vertically decaying NO_2 profile was founded on the following criteria: NO_2 originates at ground level, and undergoes photochemical conversion and dilution primarily through a first-order elimination process. A similar vertically decaying NO_2 profile shape was observed by Isaac et al. (1998) during summertime aircraft measurements conducted over Egbert, Ontario, between the elevations of 600 and 2900 m (approximately 80 km N of Toronto). These measurements demonstrated that the NO_2 concentration decreases with height by following a profile similar to the water vapour concentration, and has been predominantly associated with the dilution of ground-level emissions. Halla et al. (2011) derived composite tropospheric NO_2 VCDs by combining aircraft with ground-based in situ measurements in Ridgetown, Ontario (approximately 270 km W of Toronto). An exponentially decaying vertical NO_2 profile was assumed to determine the NO_2 vertical column present between aircraft and ground-level measurements. A significant difference was not observed when the composite NO_2 VCDs were compared to MAX-DOAS VCDs at this rural site. There are limited studies available for evaluation that derived NO_2 VCDs from stationary in situ measurements without assuming a well-mixed NO_2 vertical profile in the PBL. Previous research conducted by Schaub et al. (2006) demonstrated that in situ measurements from ground level up to 3.6 km generally obeyed a hyperbolic profile shape. This shape was applied to extract a NO_2 VCD assuming the NO_2 mixing ratio was 0.02 ppb at 8 km. Overall, the application of Eq. (2) in this paper aligns with the available research that does not rely on a CTM.

Rearranging Eq. (2) to calculate $[NO_2]_z$ shown in Eq. (3) (where z is a specified altitude) demonstrates that the concentration of $[NO_2]$ at altitude z is directly dependent on the characteristic height.

NO_2 $VCD_{in\ situ}$ were calculated on a daily basis using data averaged from 12:00 to 14:00 EST to coincide with the OMI overpass time, and hourly averaged NO_2 $VCD_{in\ situ}$ were compared to coincident MAX-DOAS measurements. Monthly averaged and diurnal profiles of H_{NO_2} and NO_2 $VCD_{in\ situ}$ were also derived.

Previous studies have investigated the positive bias associated with the CL detection of NO_2 due to the reduction of other oxidized nitrogen species (NO_z = nitric acid: HNO_3 + peroxy acetyl nitrate: $C_2H_3NO_5$ + peroxyacyl nitrates: $C_xH_yO_3NO_2$ + alkyl nitrates: $RONO_2$ + nitrous acid: HONO…) by the CL monitor's molybdenum (Mo) catalyst, which is unspecific to the reduction of NO_2 to NO. The detection of NO_z is dependent on the concentration of reactive nitrogen species at the monitoring site, the relative location of emission sources, meteorology, the conversion efficiency of NO_z species by the heated Mo surface, and their respective line losses (Lamsal et al., 2008, and references therein). The positive bias associated with the detection of NO_z exhibits seasonal and diurnal trends, reaching a maximum in the summer and during the afternoon when NO_z constitutes a larger fraction of NO_y ($NO_z + NO_x$). These trends have been associated with the photochemical production of reactive NO_z species (such as HNO_3 and PAN) alongside O_3 (Lee et al., 2011; Lamsal et al., 2008; Dunlea et al., 2007; Steinbacher et al., 2007). It was hypothesized that the bias would also vary with elevation, and thus that this positive bias should be accounted for.

The procedure reported by Boersma et al. (2009), which was based on measurements performed by Dunlea et al. (2007), was implemented to remove the influence of NO_z from CL NO_2 measurements ($[NO_2]_{CL}$) after 10:00 EST, as shown in Eq. (4), where $[NO_2]$ refers to the corrected measurement.

$$[NO_2] = [NO_2]_{CL} - [NO_z],\quad \text{where } [NO_z] = 0.1 \times \left([O_3] - [O_3]_{(10:00)}\right) \quad (4)$$

Boersma et al. (2009) applied Eq. (4) to correct CL NO_2 measurements at eight cities in Israel (2006) during the OMI overpass time (13:45 LT). This reduced the CL NO_2 measurement by an average of 8 % (0.7 ppb) during 2006. This approach was validated by using the CHIMERE CTM to determine the NO_2-to-NO_z ratio over Europe, which was typically greater than 90 % for cities exhibiting NO_2 concentrations similar to those in Israel (0–25 ppb). Boersma et al. (2009) demonstrated that the NO_2-to-NO_z ratio using Eq. (4) for January, April, July, and October was 0.99, 0.98, 0.95, and 0.98, respectively, which was in excellent

Table 3. In situ data selection criteria for the calculation of NO_2 $VCD_{in\ situ}$. Day and % of valid data refer to in situ measurements averaged during the hours of 12:00–14:00 EST to correspond with the OMI overpass time.

	In situ data selection criteria	Days	% of valid data
1	Measurement period: March 2006–March 2010	1492	
2	Valid data during March 2006–March 2010 period: NO, NO_2, $NO_x \geq 0$ ppb and $O_3 \geq 0$ ppb (10:00 EST)	1426	100
3	$NO_2 \geq 0$ ppb after applying NO_z correction	1381	97
4	Days without precipitation (rain, drizzle, or snow)	1181	83
5	NO_2 characteristic height (H_{NO_2}) ≥ 0 km	1051	74
6	[NO]/[NO_2] 445 m < [NO]/[NO_2] 10 m	817	57
7	Remove outliers (exclude average H_{NO_2} data below 10th percentile and above 90th percentile); maintain 0.23 km $\leq H_{NO_2} \leq$ 1.33 km	654	46

agreement with CHIMERE NO_2-to-NO_z ratios of 0.98, 0.96, 0.92, and 0.97.

Table 3 summarizes the inclusion criteria applied to the in situ NO_2 data during the March 2006–March 2010 period, and corresponding sample size for measurements coinciding with the OMI overpass time. Since the in situ monitors were located approximately 2.3 km apart from one another, differences in the NO_x emission characteristics at each measurement site may have influenced the observed NO_2 concentration at 10 m and 0.5 km. As shown in Table 1, the CN site experienced 24 h average weekday vehicle counts that were over 5 times greater than the DT site. Additionally, stack emissions from nearby sources may have impacted the CN measurements, resulting in a higher [NO]/[NO_2] than at ground level on some days. Therefore, an effort was made to filter data by removing hours that were strongly influenced by horizontal NO_2 gradients or did not follow a vertically decaying profile. The filtering process recognized that NO_x emitted at ground level should consist predominantly of NO and that [NO]/[NO_2] should decrease with altitude due to the oxidation of NO. Thus the 17 % of days with a greater [NO]/[NO_2] at CN than at DT were excluded, since this suggested behaviour that was inconsistent with a vertically decaying profile, making calculation of the characteristic height impossible based on measurements at the two heights. Overall, 654 of 1426 days (46 %) were maintained for comparison with OMI data. The application of all criteria in Table 3 did not selectively bias the data by season, as during the warmer months of May–August, 50 % of data was retained, while during colder months of December to March, 56 % of data was retained.

Figure 2a and b provide the frequency distribution of the NO_2 volume mixing ratio (corrected for NO_z interference – see Sect. 3.1 for results) at the DT and CN sites before and after applying selection criteria 6 and 7 in Table 3. At both measurement sites, the NO_2 volume mixing ratio retains a

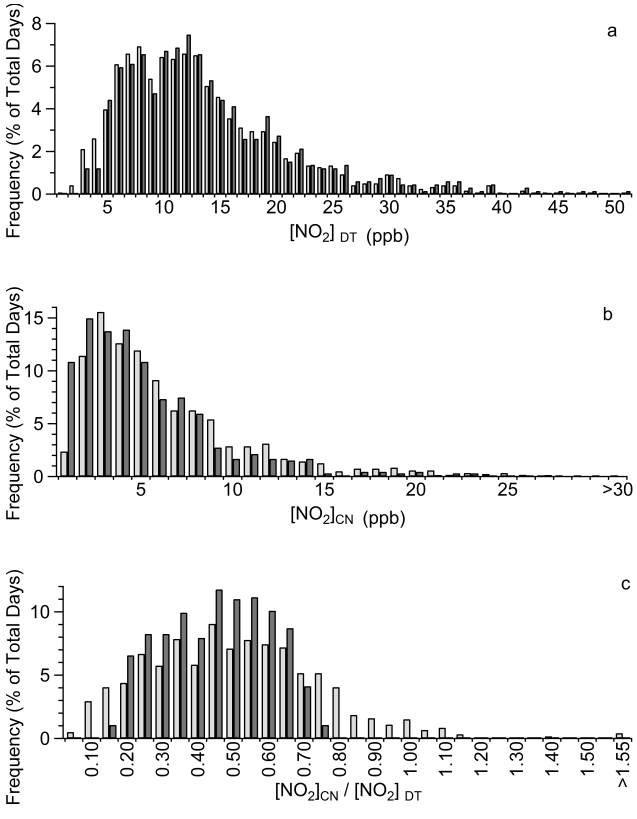

Fig. 2. (a) Frequency distribution of NO_2 DT volume mixing ratio during OMI overpass time. Light-grey bars refer to data meeting criteria 1–4 in Table 3 (Total Days = 1181) and dark-grey bars refer to data meeting all criteria in Table 3 (Total Days = 654). **(b)** Same as **(a)** but for NO_2 CN. **(c)** Same as **(a)** but for ratio of $[NO_2]_{CN}$ to $[NO_2]_{DT}$.

similar frequency distribution before and after applying these criteria. The NO_2 volume mixing ratio at DT is below 12 ppb for 54 % of the 1181 days considered (Table 3: criteria 1–4), and for 51 % of the 654 days meeting criteria 1–7 in Table 3.

Figure 2c shows the frequency distribution of the $[NO_2]_{CN}/[NO_2]_{DT}$ volume mixing ratio (corrected for NO_z interference) before and after applying selection criteria 6 and 7 in Table 3. Overall, $[NO_2]_{CN}/[NO_2]_{DT}$ is between 0.15 and 0.75 for the majority (83 %) of the 1181 days considered (Table 3: criteria 1–4), and for all data meeting criteria 1–7 in Table 3. The application of criteria 6 and 7 excludes all data (4 % of the 1181 days) with $[NO_2]_{DT}/[NO_2]_{CN} < 0.15$ and all data (13 % of the 1181 days) with $[NO_2]_{CN}/[NO_2]_{DT} > 0.75$. Furthermore, the median $[NO_2]_{CN}/[NO_2]_{DT}$ for Table 3, criteria 1–4 is 0.47, and the median for Table 3, criteria 1–7 is 0.43.

Using these criteria, the median H_{NO_2} during the hours of 12:00–14:00 EST was 0.56 km, and 58 % of data had a NO_2 characteristic height that was within 0.33 to 0.63 km. The minimum, median, and maximum NO_2 VCD averaged during the hours of 12:00–14:00 EST was 1.57×10^{15} molec cm^{-2}, 1.58×10^{16} molec cm^{-2}, and 1.18×10^{17} molec cm^{-2}, respectively. Sixty percent of data exhibited a NO_2 VCD between 1.00 and 2.00×10^{16} molec cm^{-2}.

The results presented in Fig. 2 suggest that the selection criteria in Table 3 did not systematically bias the in situ data. However, both the assumption of an exponentially decaying NO_2 vertical profile and the selection criteria are not without inherent limitations. Deviations from the assumed exponentially decaying profile shape could introduce random errors in the retrieved characteristic height, and systematic errors could also occur. While an exponentially decaying NO_2 profile shape may be a reasonable assumption during the late morning and early afternoon, it cannot account for the presence of NO_2 inversion layers at elevations between the DT and CN sites. The selection criteria in Table 3 did eliminate over half of the in situ measurements, and therefore helped decrease the likelihood of misrepresenting the NO_2 vertical profile.

The use of a consistent NO_2 vertical profile shape within the boundary layer and free troposphere was evaluated by considering the fraction of the NO_2 VCD that exceeded 2 km, which for this study was recognized as an average maximum PBL height under turbulent mixing conditions based on previous measurements conducted in southwestern Ontario (Halla et al., 2011). The rationale for this test is that the NO_2 concentration may not have decayed at a consistent rate within and above the PBL. Overall, the fraction of the NO_2 VCD above 2 km ranged from 0 to 22 %, with a median of 3 %.

2.3 MAX-DOAS instrument and NO_2 VCD retrieval algorithm

Measurements were conducted using a commercially available Mini-MAX-DOAS instrument developed by the Institute of Environmental Physics at the University of Heidelberg in collaboration with Hoffmann Messtechnik GmbH (Bobrowski and Filsinger, 2005). The MAX-DOAS instrument is equipped with a commercial crossed Czerny–Turner spectrograph (OceanOptics USB2000) having a linear resolution of 2048 pixels that cover a wavelength range of 290–433 nm. The exposure time for each spectrum was calculated such that the CCD detector reached 80 % of its saturation level. An integrated average of 1000 spectra was used to create the final spectrum. During the hours of 09:00–16:00 EST, the temporal resolution of measurements varied from approximately 1 to 1.5 min, mainly as a result of solar zenith angle. Around solar noon, a sequence of six elevation angles took approximately 8 min to survey.

"Dark current" and "offset" spectra were taken each time the instrument was set up for monitoring and subtracted from recorded spectra during analysis. The spectrometer was stabilized at 5 °C for all measurements except those conducted during the winter, when the spectrometer was maintained at −5 °C to minimize the spectrometer's exposure to temperature instability.

MAX-DOAS spectra were processed with DOASIS (Kraus, 2003) and QDOAS (Fayt et al., 2011) software to retrieve NO_2 ΔSCDs. Each spectrum was corrected for dark current and offset using DOASIS. The pixel-to-wavelength calibration was initially performed using a spectrum from a mercury lamp with known emission peaks. A calibration polynomial was generated in DOASIS based on the wavelength-to-pixel mapping of these peaks. QDOAS was then used to refine the wavelength calibration of each spectrum while simultaneously characterizing the resolution (expressed as the full width at half maximum – FWHM) of the CCD. Each spectrum was calibrated in QDOAS by performing a non-linear least-squares fit to align the structures of the measured spectrum to those of a high-resolution solar reference spectrum (0.01 nm) (Kurucz et al., 1984a) degraded to the resolution of the instrument. The resolution of the CCD (FWHM) was 0.6 nm at wavelengths greater than 380 nm.

NO_2 tropospheric ΔSCDs were retrieved from calibrated spectra by applying the DOAS technique (Platt and Stutz, 2008; Hönninger et al., 2004; Platt, 1994) using QDOAS (Fayt et al., 2011). The ΔSCD refers to the difference between the average concentration of a trace gas of interest (C) integrated along the average path length (L) traversed by photons prior to entering the spectrometer at elevation angle θ, $(\overline{CL})_\theta$ or SCD_θ, and the corresponding observation at an elevation angle of 90° within a measurement cycle, $(\overline{CL})_{90^\circ}$ or SCD_{90°, defined in Eqs. (5) and (6). Since the zenith spectrum within each measurement sequence was utilized as the

Fraunhofer reference spectrum (FRS), the influence of stratospheric absorption was removed.

$$\Delta\mathrm{SCD} = \left(\overline{\mathrm{CL}}\right)_{\theta} - \left(\overline{\mathrm{CL}}\right)_{90^\circ} \quad (5)$$

$$\Delta\mathrm{SCD} = \mathrm{SCD}_{\theta} - \mathrm{SCD}_{90^\circ} \quad (6)$$

Fit ranges reported in numerous publications (Brinksma et al., 2008; Sinreich et al., 2005; Heckel et al., 2005; Wittrock et al., 2004; Wagner et al., 2004; Friedeburg, 2003; Hönninger and Platt, 2002) were used as guides for selecting the fit range used in this study. The $NO_2\Delta$SCD was derived in the fitting window of 405–431 nm using NO_2 (294 K; Vandaele et al., 1996), HCHO (298 K; Meller and Moortgat, 2000), and O_3 (223 K; Bogumil et al., 2003) trace gas reference spectra convolved to the resolution of the instrument. The O_4 cross section (296 K; Greenblatt et al., 1990) was linearly interpolated.

Broadband absorption was accounted for by including a DOAS polynomial of order 3. A first-order offset polynomial was also used in each fit to account for stray light in the spectrometer. The Ring effect (Grainger and Ring, 1962) was accounted for by fitting measured spectra to a synthetic Ring spectrum generated in QDOAS by convolving a high-resolution solar spectrum (0.05 nm) (Kurucz et al., 1984b) with rotational Raman scattering cross sections (Fayt and van Roozendael, 2001).

Fitting errors associated with the MAX-DOAS ΔSCD are indicative of the systematic and random errors associated with the QDOAS retrieval. Systematic errors include incorrect spectral calibration, dark current and offset correction, and slit function characterization, as well as errors in the reference spectra, while random errors may be due to the presence of unknown spectral absorbance structures, and a low signal-to-noise ratio (Vlemmix et al., 2010; Fraser et al., 2009). The QDOAS fitting error generally increased as the magnitude of the ΔSCD decreased. A retrieved $NO_2\Delta$SCD of 1×10^{17} molec cm^{-2} had a relative fitting error of $\leq \pm 2$ %, while a $NO_2\Delta$SCD of 2×10^{15} molec cm^{-2} had a relative fitting error of $\leq \pm 20$ %.

Systematic errors associated with the uncertainty and temperature dependence of the NO_2 absorbance cross section have been addressed in previous studies. The measurement uncertainty associated with the NO_2 (294 K) absorption cross section is ≤ 10 % (Vandaele et al., 1998). Vlemmix et al. (2011) demonstrated that $NO_2\Delta$SCDs measured using a NO_2 absorbance cross section at 295 K should be corrected by a factor of 0.92 for an effective atmospheric temperature of 283 K (determined by considering the vertical temperature profile and the vertical distribution of NO_2 in the lower troposphere). Irie et al. (2012) reported an 11 % decrease in the NO_2 VCD by scaling it with a vertical temperature profile that decreased to 260 K at 2 km. The majority of the MAX-DOAS measurements in the current study were collected in the summer, where the characteristic height of NO_2 was typically only 500m. Any vertical variation in the NO_2 absorbance cross section within this region would have been small, as the relevant vertical variation of temperature was presumably < 5 °C. Thus this temperature sensitivity was not accounted for since, based on previous sensitivity studies, it would only have caused, on average, an error of a few percent. Certainly, some measurements were collected in March, when the average temperature was closer to 273K, and these MAX-DOAS VCDs may be overestimated by up to 10 %.

The total uncertainty associated with the $NO_2\Delta$SCD was calculated as the root sum of squares of the QDOAS fit error, absorbance cross-section accuracy, and uncertainty associated with the temperature dependence of the differential cross section. The total relative uncertainty of the $NO_2\Delta$SCD varied from 15 to 25 %. Hourly averaged $NO_2\Delta$SCDs were calculated to convert MAX-DOAS measurements to the same timescale as the available in situ measurements.

Hourly averaged geometric NO_2 VCDs were determined by applying the single-scattering approximation proposed by Hönninger et al. (2004) to MAX-DOAS $NO_2\Delta$SCDs. The NO_2 differential AMF (ΔAMF = ΔSCD/VCD) was calculated as shown in Eq. (7), and verified by using the criteria NO_2 $\mathrm{VCD}_{10^\circ} = \mathrm{VCD}_{20^\circ(\mathrm{or}30^\circ)} \pm 15$ % (Halla et al., 2011; Brinksma et al., 2008) to ensure tropospheric photon scattering occurred above the NO_2 column. Using this criterion resulted in 113 of the 169 available hourly MAX-DOAS $NO_2\Delta$SCDs being excluded. Thus, 56 h (33 %) of MAX-DOAS $NO_2\Delta$SCDs (measured at 20 or 30°) were converted to geometric VCDs during the hours of 07:00–16:00 EST for 15 days during the spring, summer, and winter collectively. Of these 56 measurements, 34 were conducted at 10 and 20°, and agreed within ± 15 %, so the 20° VCD was reported; 12 were conducted at 10 and 30°, and agreed within ± 15 %, so the 30° VCD was reported; 10 measurements were conducted at 20 and 30°, and agreed within ± 15 %, so the 30° VCD was reported. Therefore, these measurements represent the upper limit of the geometric VCD. The minimum, median, and maximum NO_2 VCD was 1.53×10^{15} molec cm^2, 1.56×10^{16} molec cm^{-2}, and 5.96×10^{16} molec cm^{-2}, during the hours of 07:00–16:00 EST, respectively. Twenty percent of data exhibited a NO_2 VCD below 5.00×10^{15} molec cm^{-2}, and 70 % of data exhibited a NO_2 VCD between 1.00 and 2.00×10^{16} molec cm^{-2}. From these time periods, 37 corresponding hours of in situ data were available for comparison.

$$\Delta\mathrm{AMF} = \left\langle \frac{1}{\sin\theta} - 1 \right\rangle \quad (7)$$

Previous studies have compared NO_2 VCDs retrieved using radiative transfer modelling to those calculated using the geometric ΔAMF (Wagner et al., 2010, 2011; Halla et al., 2011; Shaiganfar et al., 2011; Vlemmix et al., 2010). Wagner et al. (2011) converted NO_2 ΔSCDs measured at an elevation angle of 18° in south, north, and west viewing directions to NO_2 VCDs using the geometric approximation ($\mathrm{VCD}_{\mathrm{geo}}$) and the radiative transfer model McArtim ($\mathrm{VCD}_{\mathrm{RTM}}$; $\lambda = 360$ nm). The $\mathrm{VCD}_{\mathrm{geo}}/\mathrm{VCD}_{\mathrm{RTM}}$ slopes

were 0.88 ($R^2 = 0.88$), 0.96 ($R^2 = 0.96$), and 0.92 ($R^2 = 0.86$), respectively. Although no relationship between the geometric NO_2 VCD's negative bias and aerosol optical depth (AOD) was found, this bias exhibited a systematic dependency on the vertical distribution of NO_2. This systematic dependency is anticipated since the geometric ΔAMF assumes that the tropospheric NO_2 column is contained below the last scattering altitude of photons. Wagner et al. (2011) predicted that for a NO_2 column below 1000 m, the error of the geometric NO_2 VCD is typically within 20 %.

Shaiganfar et al. (2011) demonstrated that geometric NO_2 VCDs at elevation angles of 22 and 30° differed from those determined using McArtim by $\pm$20 % when assuming a 500 m vertical NO_2 box profile (AOD < 1). The geometric NO_2 VCD also exhibited a systematic dependency on relative azimuth angle (difference between the solar azimuth angle and MAX-DOAS viewing direction): the geometric VCD underestimated the true VCD at low relative azimuth angles ($\sim 0°$) and overestimated the VCD at higher relative azimuth angles ($\geq 90°$).

Vlemmix et al. (2010) demonstrated that, for relative azimuth angles greater than 30°, the difference between the geometric VCD at an elevation angle of 30° and McArtim VCD ($\lambda = 428$ nm) reaches a maximum of 25 %, and this offset is strongly a function of solar position relative to the MAX-DOAS instrument as well as AOD.

The above studies did not consider the use of validation criteria in conjunction with the geometric ΔAMF to ensure the NO_2 vertical column was contained below the last scattering altitude of photons into the MAX-DOAS detector. Halla et al. (2011) compared geometrically approximated NO_2 VCDs that met the criteria $VCD_{10°} = VCD_{30°}$ ($\pm$15 %) with those determined using the radiative transfer model McArtim ($\lambda = 413$ nm, assuming a vertical NO_2 box profile), and demonstrated geometric VCDs underestimated modelled VCDs by 8–12 %. Wagner et al. (2010) suggest that the strong agreement observed between geometrically derived NO_2 VCDs retrieved at multiple elevation angles (22 and 40°) renders the uncertainty involved in using geometrically approximated VCDs associated with aerosol loading < 15 %. Since a similar criterion for employing the geometric ΔAMF was used in this study (NO_2 $VCD_{10°} = VCD_{20°\,(\text{or } 30°)} \pm 15$ %), it is estimated that the uncertainty associated with the geometric NO_2 ΔAMF is $\leq$ 15 %. The total relative uncertainty associated with the NO_2 VCD was calculated as the root sum of squares of the random and systematic uncertainties associated with the $NO_2\Delta$SCD and the geometric $NO_2\Delta$AMF. The total relative uncertainty of the MAX-DOAS NO_2 VCD retrieval ranged from 20 to 29 %.

2.4 OMI tropospheric NO_2 columns

Dutch OMI NO_2 (DOMINO version 2.0, collection 3 level 1b) tropospheric columns were obtained from the Tropospheric Emissions Monitoring Internet Service (TEMIS) for the period of March 2006–March 2010. The DOMINO retrieval algorithm has been described in detail by Boersma et al. (2011), and is briefly reviewed here. The DOMINO product (DP) employs the DOAS algorithm (Platt, 1994) to retrieve a NO_2 slant column density (SCD) from a measured spectrum of backscattered solar radiation for the 405–465 nm wavelength range (Bucsela et al., 2006). The stratospheric NO_2 SCD is determined by assimilating the total NO_2 SCD into the TM4 global chemistry and transport model (CTM) (Dirksen et al., 2011). The stratospheric NO_2 SCD is then subtracted from the total NO_2 SCD to determine the tropospheric SCD. The AMF is obtained from the DAK radiative transfer model version 3.0 (Stammes, 2001), and relies on the a priori tropospheric NO_2 profile simulated in TM4, in addition to parameters including cloud radiance fraction, cloud pressure, surface albedo, and satellite viewing geometry. The tropospheric AMF permits the conversion of the tropospheric NO_2 SCD to the VCD (Boersma et al., 2007). The estimated uncertainty of the OMI (version 2.0) tropospheric NO_2 SCD associated with spectral fitting is 0.7×10^{15} molec cm^2, and when the uncertainty associated with the AMF is considered, this value increases to 25 % for a NO_2 tropospheric VCD measurement of 1.0×10^{15} molec cm^{-2} (Boersma et al., 2011).

The coincidence criteria used to pair OMI tropospheric NO_2 columns with independent measurements was informed by previous studies, which have constrained the sample size according to OMI cloud radiance fraction, pixel size, proximity of pixel centre to independent monitoring site, and overlap of the independent data's averaging interval with OMI overpass time (Lee et al., 2011; Hains et al., 2010; Kramer et al., 2008; Irie et al., 2008). Table 4 summarizes the criteria and coincident hours of in situ data that were used in this study. Results are presented for the 56 days of data that obeyed all criteria. The minimum, median, and maximum OMI NO_2 tropospheric VCD during these days was 3.00×10^{14} molec cm^{-2}, 6.95×10^{15} molec cm^{-2}, and 2.21×10^{16} molec cm^{-2}, respectively. Seventy-two percent of data exhibited a tropospheric NO_2 VCD below 1.00×10^{16} molec cm^{-2}.

Overall, of the 56 OMI overpasses with a cloud radiance fraction ≤ 0.3 and pixel centre within $0.1° \times 0.1°$ of DT, 10 overpasses coincided with MAX-DOAS NO_2 VCD measurements within $\pm$1 h, and 1 overpass coincided within $\pm$3 h.

Table 4. Inclusion criteria for OMI measurements.

	OMI overpass inclusion criteria	Sample size (number of days)	% of valid OMI data
1	Overpass coincides with in situ measurement that obeys criteria in Table 3	561	
2	Cloud radiance fraction ≤ 0.3	126	22
3	Pixel centre within $0.1° \times 0.1°$ (≤ 10 km) of DT (43.663° N, 79.388° W) and pixel area $\leq 600\,km^2$	56	10

Table 5. Average change in NO_2 concentration at DT and CN, characteristic height (H_{NO_2}), and vertical column density (VCD) during the hours of 12:00–14:00 EST as a result of NO_z interference correction.

Parameter	Average relative difference (%)	Average absolute difference
NO_2 DT	-8 ± 1	-0.87 ± 0.06 ppb
NO_2 CN	-12 ± 1	-0.60 ± 0.05 ppb
H_{NO_2}	0 ± 1	-0.03 ± 0.01 km
NO_2 VCD	-7 ± 1	$-5.38 \times 10^{14} \pm 2.66 \times 10^{14}$ molec cm^{-2}

3 Results and discussion

3.1 Impact of NO_z interference on chemiluminescence measurement of NO_2

Table 5 illustrates the impact of removing the NO_z interference from the average CL measurement of NO_2 during the hours of 12:00–14:00 EST. This correction reduced the CL NO_2 concentration at DT by 8 ± 1 % and at CN by 12 ± 1 %, suggesting, but not proving, that the NO_z interference associated with the CL detection of NO_2 did vary with elevation. Further, the larger NO_z interference correction at the higher elevation suggested that the correction is greater for aged air masses, consistent with observations by Boersma et al. (2009) and Steinbacher et al. (2007).

The NO_z interference varied seasonally, and had a greater impact on CL NO_2 measurements in the summer versus in the winter. During the months of December–March ($n = 222$; $T = 0.2 \pm 0.9$ °C), the NO_z correction reduced the CL NO_2 concentration at DT by 4 ± 1 % and at CN by 5 ± 1 %, while during the months of May–August ($n = 197$; $T = 22.4 \pm 0.7$ °C), the NO_z correction reduced the CL NO_2 concentration at DT by 11 ± 1 % and at CN by 21 ± 1 %. The larger NO_z interference correction at the higher elevation during the summer suggests that a greater concentration of reactive nitrogen species is present, as Dunlea et al. (2007) demonstrated that the positive and linear relationship with $[NO_z]$ and $[O_3]$ is due to the photochemical production of reactive nitrogen species alongside O_3.

The average absolute decrease in the NO_2 concentration after accounting for the NO_z interference was less than 1 ppb at both DT and CN, which is similar to observations in rural southwestern Ontario by Lee et al. (2011), who demonstrated that the median difference between the CL and true NO_2 was only 0.9 ppb. Overall, the NO_2 characteristic height decreased by an average of 30 m, and the NO_2 $VCD_{in\ situ}$ decreased by less than 1×10^{15} molec cm^{-2}.

3.2 Seasonal and diurnal variation of in situ NO_2 concentration, VCD, and characteristic height

The seasonal variation of the in situ NO_2 concentration at DT and CN is shown in Fig. 3a for data meeting criteria 1–4 in Table 3, and in Fig. 3b for data meeting all criteria in Table 3. The difference between the monthly averaged NO_2 concentrations shown in Fig. 3a versus b is not statistically significant (p value = 0.05). These results demonstrate that the monthly averaged NO_2 concentration at CN and DT determined by applying selection criteria 6 and 7 in Table 3 were representative of the concentrations determined using the original sample size of 1181 days.

The monthly averaged NO_2 concentration at both monitoring sites shown in Fig. 3b, and the monthly averaged tropospheric NO_2 VCD shown in Fig. 3c, reached a maximum during autumn and winter (November–March), and a minimum during summer (June–August). This seasonal trend is attributed to increased photolysis during the summer. The photolysis of NO_2 decreases the concentration of NO_2 relative to NO (Seinfeld and Pandis, 2006). The increased photolysis of hydroxyl radical (OH) precursor species (such as O_3) also decreases the summertime NO_2 concentration via its reaction with OH to yield nitric acid (HNO_3) (Seinfeld and Pandis, 2006; Jacob, 1999). Furthermore, an increase in anthropogenic NO_x emissions during winter months due to residential heating may have also increased the wintertime NO_2 VCD.

The seasonal variation of the in situ-derived NO_2 characteristic height is shown in Fig. 3d. These characteristic heights for NO_2 are below the expected midday PBL height, which may reach 2 km in the summer. Overall, the NO_2 characteristic height varies insignificantly within a given season. However statistically significant differences are seen when comparing winter months to spring and summer months. January and February show the greatest NO_2 characteristic heights of 0.71 ± 0.08 km and 0.78 ± 0.08 km (temperature = -2.3 ± 1.8 °C and -3.9 ± 1.4 °C, solar zenith angle $< 55°$), while minimum values are observed during the spring and summer (i.e. the characteristic height during July is 0.51 ± 0.08 km, temperature = 24.7 ± 0.9 °C, and solar zenith angle $< 33°$). This seasonal pattern for characteristic height is the opposite of that for PBL height, where maximum values occur in the summer. The increased NO_2 characteristic height during winter months indicates that

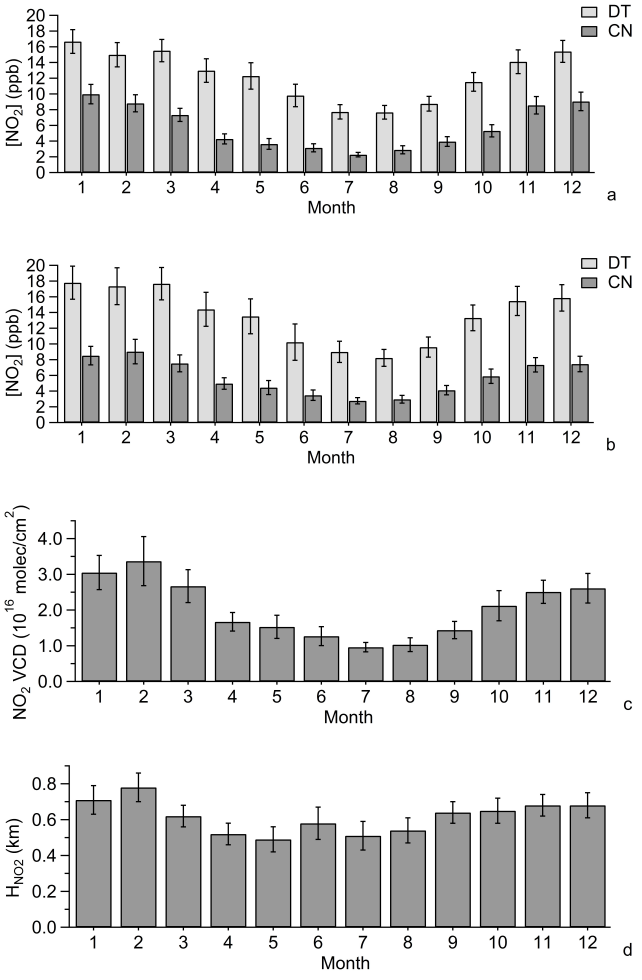

Fig. 3. (a) Monthly averaged in situ NO_2 concentration at DT and CN during the hours of 12:00–14:00 EST for data meeting criteria 1–4 in Table 3 ($n = 1181$) and **(b)** for data meeting all criteria in Table 3 ($n = 654$). **(c)** Same as **(b)** but for in situ NO_2 VCD. **(d)** Same as **(b)** but for in situ NO_2 characteristic height.

$[NO_2]_{CN}/[NO_2]_{DT}$ is greater than during the summer. This result is consistent with the increased lifetime of NO_2 during winter months, due to the decreased temperature and actinic flux, which decreases the photodissociation rate of NO_2. As a result, increased vertical homogeneity is observed. For example, $[NO_2]_{CN}/[NO_2]_{DT}$ varied from 0.52 ± 0.04 during the coldest month, February, to 0.34 ± 0.04 during the warmest month, July. More generally, the monthly average $[NO_2]_{CN}/[NO_2]_{DT}$ exhibited a negative linear dependence on the monthly average temperature, with Pearson's $R = 0.83$.

Figure 4a provides the diurnal variation of the NO_2 concentration measured at DT and CN during the autumn and winter months of December–March (average temperature = $-0.6 \pm 0.2\,^{\circ}C$), while Fig. 4b shows this diurnal variation during the spring and summer months of May–August (average temperature = $21.1 \pm 0.2\,^{\circ}C$). In both figures, the NO_2 concentration at DT exhibits a peak during the morning hours that corresponds to the evolution of the rush hour traffic period from 07:00 to 09:00 EST, and decreases during the afternoon. The loss of NO_2 to HNO_3 reaches a maximum during the afternoon due to the increased concentration of OH (Lamsal et al., 2010; Boersma et al., 2008a, 2009). The decrease in NO_2 concentration also occurs as a result of increased wind speed during afternoon hours, resulting in increased mixing, dilution, and advection of vehicular emissions. The average O_3 concentration (not shown), reflective of the OH concentration, reached a maximum during the afternoon hours. The average O_3 concentration at DT during the hours of 13:00–15:00 EST in December–March was 27.9 ± 1.2 ppb, while in May–August it was 41.7 ± 1.8 ppb. These hours generally corresponded to when the NO_2 concentration at DT reached a minimum.

During the months of December–March at 17:00 EST, the NO_2 concentration at DT began to increase in conjunction with the evening rush hour period. During the months of May–August, the NO_2 concentration remained relatively constant from 13:00 to 19:00 EST, due to higher wind speed, and in turn, dilution of emissions during the evening rush hour period. The NO_2 concentration at DT was an average of $25 \pm 1\,\%$ (5.6 ± 1 ppb) lower in the morning, and $52 \pm 2\,\%$ (4.0 ± 0.2 ppb) lower in the afternoon/evening during the warmer months than during the colder months.

The NO_2 concentration at CN in Fig. 4a and b follows a similar profile as the NO_2 concentration at DT. In both figures, the morning rush hour peak is not as pronounced as at DT, likely due to the dilution of vehicle emissions with increasing altitude. The NO_2 concentration at CN also reaches a minimum during the afternoon when the O_3, and presumably OH, concentration at CN reaches a maximum. The average O_3 concentration at CN during the hours of 13:00–15:00 EST in December–March was 33.2 ± 1.1 ppb (19 % greater than at DT), while in May–August it was 47.8 ± 4.7 ppb (15 % greater than at DT). The NO_2 concentration at CN was an average of $27 \pm 8\,\%$ (2.4 ± 0.2 ppb) lower in the morning, and $52 \pm 2\,\%$ (4.0 ± 0.1 ppb) lower in the afternoon/evening during the warmer months than during the colder months.

Figure 4c shows the diurnal variation of the NO_2 characteristic height, and $[NO_2]_{CN}/[NO_2]_{DT}$ during the months of December–March, while Fig. 4d shows this diurnal variation during the months of May–August. Both H_{NO_2} and $[NO_2]_{CN}/[NO_2]_{DT}$ follow a similar profile since $[NO_2]_{CN}/[NO_2]_{DT}$ was used to derive H_{NO_2}. As shown in Eq. (2), an increase in $[NO_2]_{CN}/[NO_2]_{DT}$ results in an increased H_{NO_2}.

The NO_2 characteristic height during the months of December–March exhibited a diurnal trend that is similar to the evolution of the PBL, which increases during the morning hours and peaks in the afternoon (Jacob, 1999). The NO_2 characteristic height (and $[NO_2]_{CN}/[NO_2]_{DT}$) is an average of 0.5 ± 0.3 km (0.39 ± 0.02) during the hours of

07:00–10:00 EST, and reaches an average of 0.65 ± 0.01 km (0.47 ± 0.01) during the hours of 11:00–17:00 EST.

During the months of May–August, a statistically significant difference for both the hourly averaged H_{NO_2} and $[NO_2]_{CN}/[NO_2]_{DT}$ was not witnessed between the hours of 08:00 and 19:00 EST. The average characteristic height during these hours was 0.56 ± 0.01 km – 14 % lower than the average maximum characteristic height in December–March, while the average $[NO_2]_{CN}/[NO_2]_{DT}$ during these hours was 0.41 ± 0.01 – 13 % lower than the average maximum ratio in December–March. These results demonstrate that the vertical distribution of NO_2 within 0.5 km during the period of spring–summer does not follow the typical diurnal profile of the convective PBL, which is typically higher during warmer months than colder months.

Previous research using radiosonde measurements has demonstrated that the height of the PBL in southern Ontario (43.682° N, 79.612° W) is an average of 1.5 km during the summer. An increased PBL height during the summer is directly related to the increase in solar radiation and surface heat flux (Ning and Yap, 1986). The NO_2 characteristic heights shown in Fig. 4d are over 60 % lower than these radiosonde measurements of the PBL height, which suggest they cannot be considered representative of the diurnal evolution of the PBL. Overall, Fig. 4d shows that assuming a well-mixed NO_2 concentration within the PBL will lead to an overestimate of the tropospheric NO_2 VCD.

Figure 4e provides the diurnal variation of the in situ NO_2 VCD during the months of December–March, while Fig. 4f shows this diurnal variation during the months of May–August. The diurnal profile shown in both figures closely replicate the diurnal profile of the NO_2 concentration at DT ($R = 0.87$ and $R = 0.93$, respectively). During the afternoon and evening hours, the NO_2 VCD is at least 2 times greater during the months of December–March versus May–August. This is due to both the increased concentration of NO_2 DT and the increased $[NO_2]_{CN}/[NO_2]_{DT}$ during the colder months. Since the diurnal trends presented in Fig. 4e and f rely on the assumption of an exponentially decaying vertical NO_2 profile, the presence of NO_2 inversion layers at elevations between the DT and CN sites could result in an underestimation of the VCD at times, especially during the winter morning hours.

3.3 Comparison between in situ and remotely sensed NO_2 VCDs

Figure 5 shows the linear regression of the OMI versus in situ tropospheric NO_2 VCD. Linear regression was performed using data meeting all OMI overpass criteria in Table 4. The OMI tropospheric NO_2 VCD exhibits a negative bias of 58 % when compared to the in situ NO_2 VCD and good correlation with a Pearson's R value of 0.81. These results are consistent with the spatial footprint represented by these two types of measurements. The in situ monitors measure a point-location "near-roadside" NO_2 column, while the OMI NO_2 VCD reflects an average over the spatially heterogeneous Greater Toronto Area, consisting of roads, residential neighbourhoods, and Lake Ontario.

Figure 6 shows the linear regression results of the MAX-DOAS versus in situ tropospheric NO_2 VCD, and although good agreement is seen (Pearson's $R = 0.72$), the MAX-DOAS NO_2 VCD is only 42 % of the corresponding value determined using the in situ monitors. The difference between the MAX-DOAS versus in situ-derived NO_2 VCD suggests that differences in the geographic footprint surveyed by each instrument impacted the results. As summarized in Table 2, much of the MAX-DOAS path length was over Lake Ontario during campaigns A, D, and E; was facing east for campaign C; and was located 65 m a.g.l. in campaigns C and D. During all campaigns, the MAX-DOAS instrument's path length was also influenced by the NO_2 concentration in residential areas in the downtown core.

The spatial heterogeneity of the NO_2 concentration across Toronto was evaluated by Jerrett et al. (2007, 2009). Passive sampling measurements of NO_2 concentration at 143 sites in the early autumn of 2002 and spring of 2004 were used in conjunction with land-use regression modelling to derive a NO_2 surface concentration map. Despite changes in absolute NO_2 concentration between seasons, overall spatial patterns remained similar: NO_2 exhibited higher concentrations in the west (> 20 ppb), and lower concentrations in the east (10–15 ppb). The downtown core and areas near major highways also exhibited high NO_2 concentrations (> 30 ppb). The MAX-DOAS path length over mainland Toronto consists of a combination of urban background and roadside NO_2 concentrations, and the MAX-DOAS NO_2 VCD is dependent on these gradients.

Figure 7 shows the linear regression results of OMI versus MAX-DOAS tropospheric NO_2 VCDs. A good agreement is seen between the measurement techniques, which have a Pearson's R value of 0.80. The slope presented in Fig. 7 derived using linear regression is 0.93 ± 0.11, or if weighted orthogonal distance regression is applied, then this slope is 0.74 ± 0.16. These slopes are in agreement when their respective errors are considered, and in both cases the slope is not significantly different from 1. Of the 11 available comparison days, 8 OMI and MAX-DOAS measurements agree when the respective uncertainties of each measurement are considered. The results presented in Fig. 7 suggest that MAX-DOAS and OMI measurements both "look at" similar mixes of the spatial heterogeneity in NO_2 concentrations created by the unpolluted regions over Lake Ontario and polluted regions over the city. Thus this finding is indirectly consistent with the majority of previous studies which suggest that OMI exhibits a positive bias over rural (unpolluted) MAX-DOAS measurement sites, and a negative bias over urban (polluted) MAX-DOAS measurement sites (Shaiganfar et al., 2011; Halla et al., 2011; Wagner et al., 2010; Kramer et al., 2008; Brinksma et al., 2008; Celarier et al., 2008). In

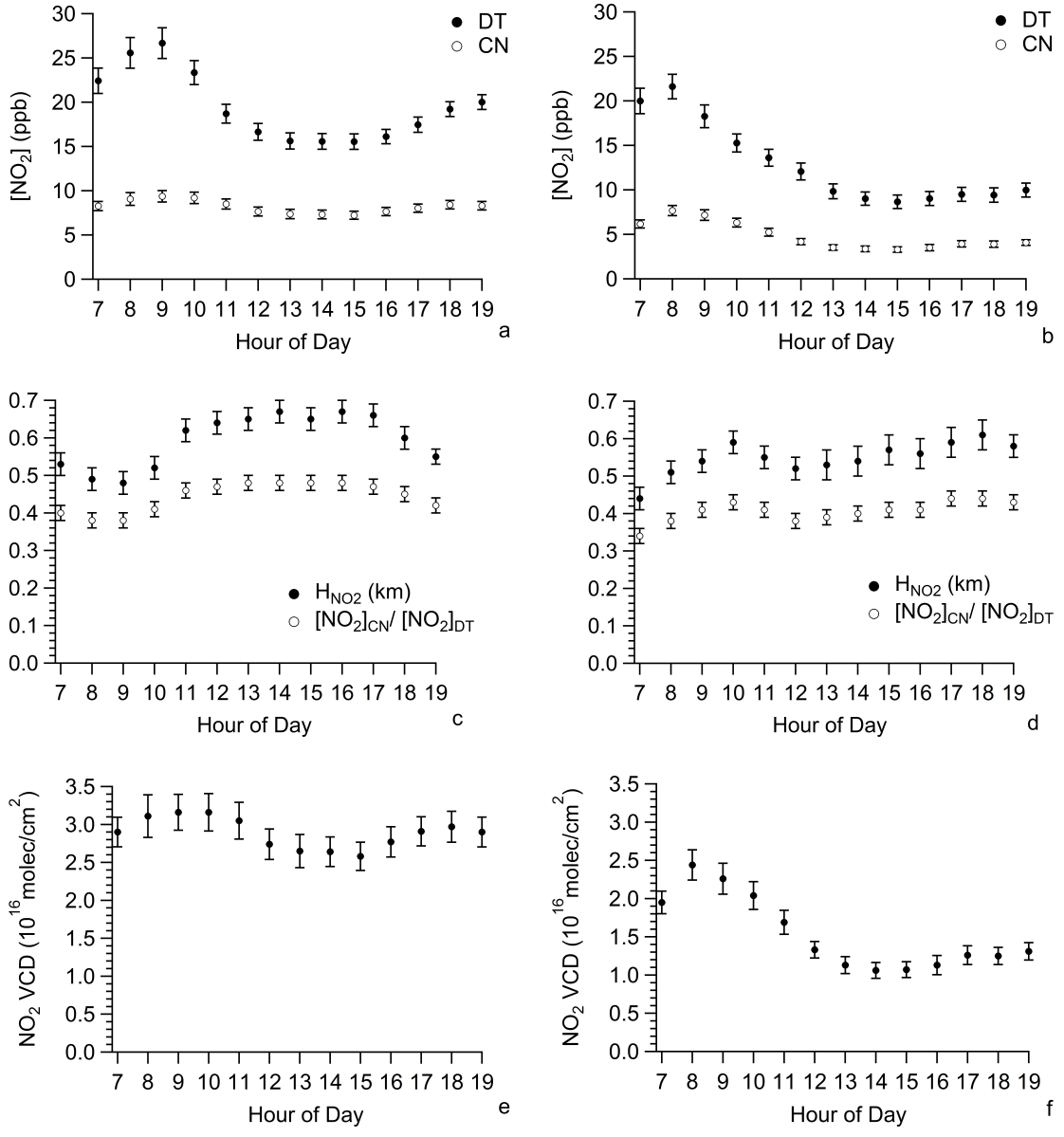

Fig. 4. (a) Diurnal profile of $[NO_2]$ at DT and CN during the months of December–March and **(b)** May–August. **(c)** Diurnal profile of H_{NO_2} and $[NO_2]_{CN}/[NO_2]_{DT}$ during the months of December–March and **(d)** May–August. **(e)** Diurnal profile of NO_2 VCD during the months of December–March and **(f)** May–August. Plots were derived by applying all criteria in Table 3 during the hours of 07:00–19:00 EST for hourly averaged data having H_{NO_2} within 10th to 90th percentile.

the heterogeneous polluted and unpolluted environment of the current study, the two remote sensing methods yield similar vertical columns. More importantly, when these ground- and satellite-based measurement methods "look at" the same mixture of environments, then they agree, providing reassurance in the validity of the measurements produced by each method.

4 Conclusions

In situ measurements of NO_2 in an urban environment were compared with remotely sensed satellite, and multi-axis differential optical absorption spectroscopy (MAX-DOAS), tropospheric NO_2 vertical column densities (VCDs). The chemiluminescence measurements were first corrected for the influence of NO_z, which reduced the NO_2 concentrations near ground level and at 445 m by an average of 8 ± 1 % and 12 ± 1 %, respectively. The absolute decrease in the

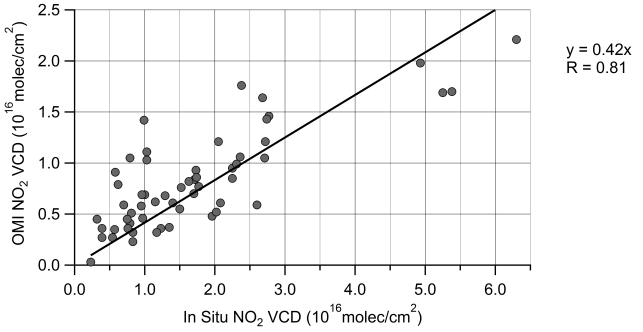

Fig. 5. Linear regression of OMI versus in situ tropospheric NO_2 VCD for data meeting all OMI overpass criteria in Table 4.

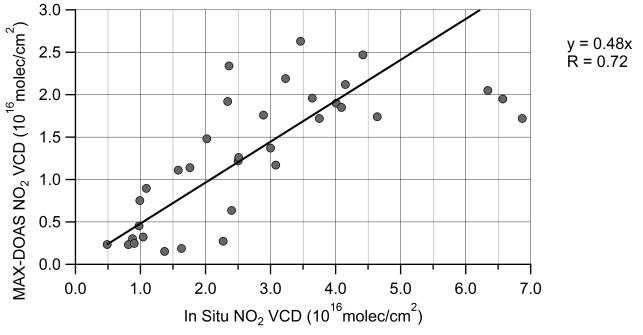

Fig. 6. Linear regression of MAX-DOAS versus in situ tropospheric NO_2 VCD.

chemiluminescence NO_2 measurements as a result of this correction was less than 1 ppb.

The monthly averaged ratio of the NO_2 concentration at 0.5 to 0.01 km varied seasonally, and exhibited a negative linear dependence on the monthly average temperature, with Pearson's $R = 0.83$. During the coldest month, February, this ratio was 0.52 ± 0.04, while during the warmest month, July, this ratio was 0.34 ± 0.04, thereby demonstrating that NO_2 is not well mixed in the PBL.

The NO_2 characteristic height during the months of December–March exhibited a diurnal trend that was similar but much weaker than the evolution of the PBL, while during the months of May–August, a statistically significant difference for both the hourly averaged H_{NO_2} and $[NO_2]_{CN}/[NO_2]_{DT}$ was not witnessed between the hours of 08:00 and 19:00 EST. The average characteristic height during these hours was 0.56 ± 0.01 km – 14 % lower than the average maximum characteristic height in December–March. These results demonstrate that the vertical distribution of NO_2 within 0.5 km during the period of spring–summer does not follow the typical diurnal profile of the convective PBL, which is generally higher during warmer months than colder months. Although NO_2 profile inversions at elevations between the DT and CN sensors could not be detected using the method employed, overall, the presented results suggest that

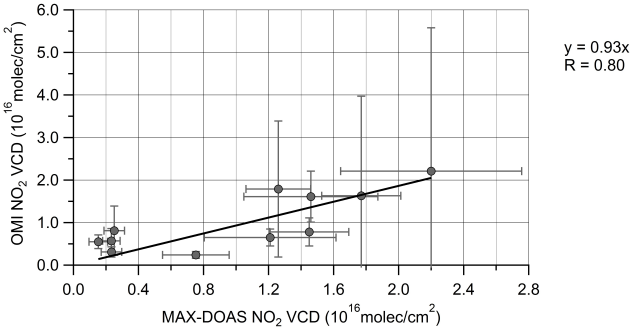

Fig. 7. Linear regression of OMI versus MAX-DOAS tropospheric NO_2 VCD.

assuming a well-mixed NO_2 concentration within the PBL will lead to an overestimate of the NO_2 VCD.

Strong correlation was observed between the remotely sensed and in situ NO_2 VCDs (Pearson's R value ranging from 0.72 to 0.81). However, the in situ VCDs were 52 to 58 % greater than the remotely sensed columns due to horizontal spatial heterogeneity, and possibly random and systematic errors associated with each VCD measurement technique. Notably, the in situ VCDs were based on an assumed exponential vertical profile. The in situ NO_2 VCD were representative of a local NO_2 column in a polluted near-road environment, while the remotely sensed (MAX-DOAS and OMI) VCDs were representative of a spatially heterogeneous region, which included the downtown city core, residential neighbourhoods, and Lake Ontario. Overall, the reasonable agreement between the VCD values determined by the three distinct methods increased confidence in the validity of the values provided by each of the measurement techniques.

Acknowledgements. The authors thank the Ontario Ministry of the Environment for providing the in situ data, and Environment Canada for funding the MAX-DOAS instrument and providing operational support for R. D'Souza. The authors acknowledge Michel Van Roozendael and Caroline Fayt of the Belgian Institute for Space Aeronomy for the development of QDOAS. The authors acknowledge Stephen Kraus and Thomas Lehmann of the University of Heidelberg's Institute for Environmental Physics for the development of DOASIS. The authors acknowledge the free use of OMI tropospheric NO_2 vertical column densities from the Tropospheric Emission Monitoring Internet Service (TEMIS). The authors express their thanks to colleagues of SOCAAR, the University of Toronto's Atmospheric Physics Department, and York University's Centre for Atmospheric Chemistry for ongoing collaboration and discussions. Finally, the authors acknowledge the contribution of Sarah Basma, who helped collect the MAX-DOAS Centre Island data.

Edited by: F. Boersma

References

Andersen, Z. J., Hvidberg, M., Jensen, S. S., Ketzel, M., Loft, S., Sørensen, M., Tjønneland, A., Overvad, K., and Raaschou-Nielsen, O.: Chronic obstructive pulmonary disease and long-term exposure to traffic-related air pollution: a cohort study, Am. J. Respir. Crit. Care Med., 183, 455–461, 2011.

Bechle, M. J., Millet, D. B., and Marshall, J. D.: Remote sensing of exposure to NO_2: Satellite versus ground-based measurement in a large urban area, Atmos. Environ., 69, 343–353, 2013.

Beckerman, B., Jerrett, M., Brook, J. R., Verma, D. K., Arain, M. A., and Finkelstein, M. A.: Correlation of nitrogen dioxide with other traffic pollutants near a major expressway, Atmos. Environ., 42, 275–290, 2008.

Bobrowski, N. and Filsinger, F., Mini MAX-DOAS – an Introduction, Institute of Environmental Physics, University of Heidelberg, Heidelberg, 2005.

Boersma, K. F., Eskes, H. J., Veefkind, J. P., Brinksma, E. J., van der A, R. J., Sneep, M., van den Oord, G. H. J., Levelt, P. F., Stammes, P., Gleason, J. F., and Bucsela, E. J.: Near-real time retrieval of tropospheric NO_2 from OMI, Atmos. Chem. Phys., 7, 2103–2118, doi:10.5194/acp-7-2103-2007, 2007.

Boersma, K. F., Jacob, D. J., Eskes, H. J., Pinder, R. W., Wang, J., and van der A., R.: Intercomparison of SCIAMACHY and OMI tropospheric NO_2 columns: Observing the diurnal evolution of chemistry and emissions from space, J. Geophys. Res.-Atmos., 113, D16S26, doi:10.1029/2007JD008816, 2008a.

Boersma, K. F., Jacob, D. J., Bucsela, E. J., Perring, A. E., Dirksen, R., van der A, R. J., Yantosca, R. M., Park, R. J., Wenig, M. O., Bertram, T. H., and Cohen, R. C.: Validation of OMI tropospheric NO_2 observations during INTEX-B and application to constrain NO_x emissions over the Eastern United States and Mexico, Atmos. Environ., 42, 4480–4497, doi:10.1016/j.atmosenv.2008.02.004, 2008b.

Boersma, K. F., Jacob, D. J., Trainic, M., Rudich, Y., DeSmedt, I., Dirksen, R., and Eskes, H. J.: Validation of urban NO_2 concentrations and their diurnal and seasonal variations observed from the SCIAMACHY and OMI sensors using in situ surface measurements in Israeli cities, Atmos. Chem. Phys., 9, 3867–3879, doi:10.5194/acp-9-3867-2009, 2009.

Boersma, K. F., Eskes, H. J., Dirksen, R. J., van der A, R. J., Veefkind, J. P., Stammes, P., Huijnen, V., Kleipool, Q. L., Sneep, M., Claas, J., Leitão, J., Richter, A., Zhou, Y., and Brunner, D.: An improved tropospheric NO_2 column retrieval algorithm for the Ozone Monitoring Instrument, Atmos. Meas. Tech., 4, 1905–1928, doi:10.5194/amt-4-1905-2011, 2011.

Bogumil, K., Orphal, J., Homann, T., Voigt, S., Spietz, P., Fleischmann, O. C., Vogel, A., Hartmann, M., Kromminga, H., Bovensmann, H., Frerick, J., and Burrows, J. P.: Measurements of Molecular Absorption Spectra with the SCIAMACHY Pre-Flight Model: Instrument Characterization and Reference Data for Atmospheric Remote-Sensing in the 230–2380 nm Region, J. Photochem. Photobiol. A., 157, 167–184, 2003.

Brinksma, E. J., Pinardi, G., Volten, H., Braak, R., Richter, A., Schoenhardt, A., Van Roozendael, M., Fayt, C., Hermans, C., Dirksen, R. J., Vlemmix, T., Berkhout, A. J. C., Swart, D. P. J., Oetjes, H., Wittrock, F., Wagner, T., Ibrahim, O., de Leeuw, G., Moerman, M., Curier, R. L., Celarier, E. A., Cede, A., Knap, W. H., Veefkind, J. P., Eskes, H. J., Allaart, M., Rothe, R., Piters, A. J. M., and Levelt, P. F.: The 2005 and 2006 DANDELIONS NO_2 and aerosol intercomparison campaigns, J. Geophys. Res.-Atmos., 113, D16S46, doi:10.1029/2007JD008988, 2008.

Bucsela, E. J., Celarier, E. A., Wenig, M. O., Gleason, J. F., Veefkind, J. P., Boersma, K. F., and Brinksma, E. J.: Algorithm for NO_2 vertical column retrieval from the Ozone Monitoring Instrument, IEEE T. Geosci. Remote, 44, 1245–1258, doi:10.1109/TGRS.2005.863715, 2006.

Bucsela, E. J., Perring, A. E., Cohen, R. C., Boersma, K. F., Celarier, E. A., Gleason, J. F., Wenig, M. O., Bertram, T. H., Wooldridge, P. J., Dirksen, R., and Veefkind, J. P.: Comparison of tropospheric NO_2 from in-situ aircraft measurements with near-real time and standard product data from OMI, J. Geophys. Res.-Atmos., 113, D16S31, doi:10.1029/2007JD008838, 2008.

Celarier, E. A., Brinksma, E. J., Gleason, J. F., Veefkind, J. P., Cede, A., Herman, J. R., Ionov, D., Goutail, F., Pommereau, J. P., Lambert, J. C., van Roozendael, M., Pinardi, G., Wittrock, F., Schonhardt, A., Richter, A., Ibrahim, O. W., Wagner, T., Bojkov, B., Mount, G., Spinei, E., Chen, C. M., Pongetti, T. J., Sander, S. P., Bucsela, E. J., Wenig, M. O., Swart, D. P. J., Volten, H., Kroon, M., and Levelt, P. F.: Validation of Ozone Monitoring Instrument nitrogen dioxide columns, J. Geophys. Res.-Atmos., 113, D15S15, doi:10.1029/2007JD008908, 2008.

Clements, A. L., Jia, Y., Denbleyker, A., McDonald-Buller, E., Fraser, M. P., Allen, D. T., Collins, D. R., Michel, E., Pudota, J., Sullivan, D., and Zhu, Y.: Air pollutant concentrations near three Texas roadways, part II: Chemical characterization and transformation of pollutants, Atmos. Environ., 43, 4523–4534, 2009.

Dirksen, R. J., Boersma, K. F., Eskes, H. J., Ionov, D. V., Bucsela, E. J., Levelt, P. F., and Kelder, H. M.: Evaluation of stratospheric NO_2 retrieved from the Ozone Monitoring Instrument: Intercomparison, diurnal cycle, and trending, J. Geophys. Res., 116, D08305, doi:10.1029/2010JD014943, 2011.

Duncan, B. N., Yoshida, Y., Olson, J. R., Sillman, S., Martin, R. V., Lasmal, L., Hu, Y., Pickering, K. E., Retscher, C., Allen, D. J., and Crawford, J. H.: Application of OMI observations to a space-based indicator of NO_x and VOC controls on surface ozone formation, Atmos. Environ., 44, 2213–2223, doi:10.1016/j.atmosenv.2010.03.010, 2010.

Dunlea, E. J., Herndon, S. C., Nelson, D. D., Volkamer, R. M., San Martini, F., Sheehy, P. M., Zahniser, M. S., Shorter, J. H., Wormhoudt, J. C., Lamb, B. K., Allwine, E. J., Gaffney, J. S., Marley, N. A., Grutter, M., Marquez, C., Blanco, S., Cardenas, B., Retama, A., Ramos Villegas, C. R., Kolb, C. E., Molina, L. T., and Molina, M. J.: Evaluation of nitrogen dioxide chemiluminescence monitors in a polluted urban environment, Atmos. Chem. Phys., 7, 2691–2704, doi:10.5194/acp-7-2691-2007, 2007.

Environment Canada – EC: Criteria Air Contaminants and Related Pollutants, http://www.ec.gc.ca/air/default.asp?lang=En&n=7C43740B-1, last access: 18 October 2013.

Fayt, C. and Van Roozendael, M.: WinDOAS 2.1 Software User Manual, Belgian Institute For Space Aeronomy, Brussels, Belgium, 2001.

Fayt, C., De Smedt, I., Letocart, V., Merlaud, A., Pinardi, G., and Van Roozendael, M.: QDOAS Software user manual version 1.00, Belgian Institute For Space Aeronomy, Brussels, Belgium, 2011.

Fraser, A., Adams, C., Drummond, J. R., Goutail, F., Manney, G., and Strong, K.: The Polar Environment Atmospheric Research Laboratory UV-Visible Ground-Based Spectrometer: First Measurements of O_3, NO_2, BrO, and OClO Columns, J. Quant. Spectrosc. Ra., 110, 986–1004, doi:10.1016/j.jqsrt.2009.02.034, 2009.

Friedeburg, C.: Derivation of Trace Gas Information combining Differential Trace Gas Absorption Spectroscopy with Monte Carlo Radiative Transfer Modeling, PhD Dissertation, University of Heidelberg, Heidelberg, Germany, 2003.

Grainger, J. F. and Ring, J., Anomalous Fraunhofer line profiles, Nature, 193, p. 762, doi:10.1038/193762a0, 1962.

Greenblatt, G. D., Orlando, J. J., Burkholder, J. B., and Ravishankara, A. R.: Absorption measurements of oxygen between 330 and 1140 nm, J. Geophys. Res.-Atmos., 95, 18577–18582, doi:10.1029/JD095iD11p18577, 1990.

Hains, J. C., Boersma, K. F., Kroon, M., Dirksen, R. J., Cohen, R. C., Perring, A. E., Bucsela, E., Volten, H., Swart, D. P. J., Richter, A., Wittrock, F., Schonhardt, A., Wagner, T., Ibrahim, O. W., van Roozendael, M., Pinardi, G., Gleason, J. F., Veefkind, J. P., and Levelt, P.: Testing and improving OMI DOMINO tropospheric NO_2 using observations from the DANDELIONS and INTEX-B validation campaigns, J. Geophys. Res.-Atmos., 115, D05301, doi:10.1029/2009JD012399, 2010.

Halla, J. D., Wagner, T., Beirle, S., Brook, J. R., Hayden, K. L., O'Brien, J. M., Ng, A., Majonis, D., Wenig, M. O., and McLaren, R.: Determination of tropospheric vertical columns of NO_2 and aerosol optical properties in a rural setting using MAX-DOAS, Atmos. Chem. Phys., 11, 12475–12498, doi:10.5194/acp-11-12475-2011, 2011.

Heckel, A., Richter, A., Tarsu, T., Wittrock, F., Hak, C., Pundt, I., Junkermann, W., and Burrows, J. P.: MAX-DOAS measurements of formaldehyde in the Po-Valley, Atmos. Chem. Phys., 5, 909–918, doi:10.5194/acp-5-909-2005, 2005.

Hönninger, G., von Friedeburg, C., and Platt, U.: Multi axis differential optical absorption spectroscopy (MAX-DOAS), Atmos. Chem. Phys., 4, 231–254, doi:10.5194/acp-4-231-2004, 2004.

Hönninger, G. and Platt, U., Observations of BrO and its vertical distribution during surface ozone depletion at Alert, Atmos. Environ., 36, 2481–2489, doi:10.1016/S1352-2310(02)00104-8, 2002.

Huijnen, V., Williams, J., van Weele, M., van Noije, T., Krol, M., Dentener, F., Segers, A., Houweling, S., Peters, W., de Laat, J., Boersma, F., Bergamaschi, P., van Velthoven, P., Le Sager, P., Eskes, H., Alkemade, F., Scheele, R., Nédélec, P., and Pätz, H.-W.: The global chemistry transport model TM5: description and evaluation of the tropospheric chemistry version 3.0, Geosci. Model Dev., 3, 445–473, doi:10.5194/gmd-3-445-2010, 2010.

Irie, H., Kanaya, Y., Akimoto, H., Tanimoto, H., Wang, Z., Gleason, J. F., and Bucsela, E. J.: Validation of OMI tropospheric NO_2 column data using MAX-DOAS measurements deep inside the North China Plain in June 2006: Mount Tai Experiment 2006, Atmos. Chem. Phys., 8, 6577–6586, doi:10.5194/acp-8-6577-2008, 2008.

Irie, H., Takashima, H., Kanaya, Y., Boersma, K. F., Gast, L., Wittrock, F., Brunner, D., Zhou, Y., and Van Roozendael, M.: Eight-component retrievals from ground-based MAX-DOAS observations, Atmos. Meas. Tech., 4, 1027–1044, doi:10.5194/amt-4-1027-2011, 2011.

Irie, H., Boersma, K. F., Kanaya, Y., Takashima, H., Pan, X., and Wang, Z. F.: Quantitative bias estimates for tropospheric NO_2 columns retrieved from SCIAMACHY, OMI, and GOME-2 using a common standard for East Asia, Atmos. Meas. Tech., 5, 2403–2411, doi:10.5194/amt-5-2403-2012, 2012.

Isaac, G. A., Banic, C. M., Leaitch, W. R., Anlauf, K. G., Couture, M. D., Liu, P. S. K., Macdonald, A. M., MacQuarrie, K. I. A., Puckett, K. J., and Wiebe, H. A.: Vertical profiles and horizontal transport of atmospheric aerosols and trace gases over central Ontario, J. Geophys. Res., 103, 22015–22037, doi:10.1029/98JD01727, 1998.

Jacob, D. J.: Introduction to Atmospheric Chemistry, Princeton University Press, Princeton, N.J., 1999.

Jerrett, M., Arain, M. A., Kanaroglou, P., Beckerman, B., Crouse, D., Gilbert, N. L., and Brook, J. R., Finkelstein, N., and Finkelstein, M. M.: Modeling the intraurban variability of ambient traffic pollution in Toronto, Canada, J. Toxicol. Environ. Health A, 70, 200–212, 2007.

Jerrett, M., Finkelstein, M. M., Brook, J. R., Altaf Arain, M., Kanaroglou, P., Stieb, D. M., Gilbert, N. L., Verma, D., Finkelstein, N., Chapman, K. R., and Sears, M. R.: A Cohort Study of Traffic-Related Air Pollution and Mortality in Toronto, Ontario, Canada, Environ. Health Perspect., 117, 772–777, doi:10.1289/ehp.11533, 2009.

Kramer, L. J., Leigh, R. J., Remedios, J. J., and Monks, P. S.: Comparison of OMI and ground-based in situ and MAXDOAS measurements of tropospheric nitrogen dioxide in an urban area, J. Geophys. Res.-Atmos., 113, D16S39, doi:10.1029/2007JD009168, 2008.

Kraus S.: DOASUI 3.2.3268.34613, Institute of Environmental Physics – University of Heidelberg in cooperation with Hoffmann Messtichnik GmbH, www.iup.uni-heidelberg.de/bugtracker/projects/doasis/download.php/ (last access: 18 October 2013), 2003.

Kurucz, R. L., Furenlid, I., Brault, J., and Testerman, L.: Solar flux atlas from 296 nm to 1300 nm, Resolution: 0.01 nm, National Solar Observatory Atlas No. 1, Office of University publisher, Harvard University, Cambridge, 1984a.

Kurucz, R. L., Furenlid, I., Brault, J., and Testerman, L.: Solar flux atlas from 296 nm to 1300 nm, Resolution: 0.05 nm, National Solar Observatory Atlas No. 1, Office of University publisher, Harvard University, Cambridge, 1984b.

Lamsal, L. N., Martin, R. V., van Donkelaar, A., Steinbacher, M., Celarier, E. A., Bucsela, E., Dunlea, E. J., and Pinto, J. P.: Ground-level nitrogen dioxide concentrations inferred from the satellite-borne Ozone Monitoring Instrument, J. Geophys. Res.-Atmos., 113, D16308, doi:10.1029/2007JD009235, 2008.

Lamsal, L. N., Martin, R. V., van Donkelaar, A., Celarier, E. A., Bucsela, E. J., Boersma, K. F., Dirksen, R., Luo, C., and Wang, Y.: Indirect validation of tropospheric nitrogen dioxide retrieved from the OMI satellite instrument: insight into the seasonal variation of nitrogen oxides at northern midlatitudes, J. Geophys. Res.-Atmos., 115, D05302, doi:10.1029/2009JD013351, 2010.

Lee, C. J., Brook, J. R., Evans, G. J., Martin, R. V., and Mihele, C.: Novel application of satellite and in-situ measurements to map surface-level NO_2 in the Great Lakes region, Atmos. Chem. Phys., 11, 11761–11775, doi:10.5194/acp-11-11761-2011, 2011.

Levelt, P., van den Oord, G., Dobber, M., Malkki, A., Visser, H., de Vries, J., Stammes, P., Lundell, J., and Saari, H.: The Ozone Monitoring Instrument, IEEE T. Geosci. Remote, 44, 1093–1101, doi:10.1109/TGRS.2006.872333, 2006.

McAdam, K., Steer, P., and Perrotta, K.: Using continuous sampling to examine the distribution of traffic related air pollution in proximity to a major road, Atmos. Environ., 45, 2080–2086, doi:10.1016/j.atmosenv.2011.01.050, 2011.

Mei, L., Xue, Y., de Leeuw, G., Guang, J., Wang, Y., Li, Y., Xu, H., Yang, L., Hou, T., He, X., Wu, C., Dong, J., and Chen, Z.: Integration of remote sensing data and surface observations to estimate the impact of the Russian wildfires over Europe and Asia during August 2010, Biogeosciences, 8, 3771–3791, doi:10.5194/bg-8-3771-2011, 2011.

Meller, R. and Moortgat, G. K.: Temperature dependence of the absorption cross sections of formaldehyde between 223 and 323 K in the wavelength range 225–375 nm, J. Geophys. Res.-Atmos., 105, 7089–7101, doi:10.1029/1999JD901074, 2000.

MOE – Ontario Ministry of the Environment: Air Quality in Ontario: Current Pollutant Concentrations, http://www.airqualityontario.com/history/summary.php (last access: 18 October 2013), 2010a.

MOE – Ontario Ministry of the Environment: What is the Air Quality Index?, http://www.airqualityontario.com/science/aqi_description.php (last access: 18 October 2013), 2010b.

MOE – Ontario Ministry of the Environment: Air Quality in Ontario 2009 Report, http://www.ene.gov.on.ca/environment/en/resources/STDPROD_081227.html (last access: 18 October 2013), 2011.

Nafstad, P., Haheim, L. L., Oftedal, B., Gram, F., Holme, I., Hjermann, I., and Leren, P.: Lung cancer and air pollution: a 27 year follow up of 16 209 Norwegian men, Thorax, 58, 1071–107, 2003.

Ning, D. T. and Yap, D.: Climatology of convective boundary-layer parameters over Ontario, Canada, Atmos. Environ., 20, 2315–2323, doi:10.1016/0004-6981(86)90062-4, 1986.

Ordóñez, C., Richter, A., Steinbacher, M., Zellweger, C., Nüß, H., Burrows, J. P., and Prévôt, A. S. H.: Comparison of 7 years of satellite-borne and ground-based tropospheric NO_2 measurements around Milan, Italy, J. Geophys. Res.-Atmos., 111, D05310, doi:10.1029/2005JD006305, 2006.

Pereira, G., Cook, A., De Vos, A. J. B. M., and Holman, D.: A case-crossover analysis of traffic-related air pollution and emergency department presentations for asthma in Perth, Western Australia, Med. J. Aust., 193, 511–514, 2010.

Petritoli, A., Bonasoni, P., Giovanelli, G., Ravegnani, F., Kostadinov, I., Bortoli, D., Weiss, A., Schaub, D., Richter, A., and Fortezza, F.: First comparison between ground-based and satellite-borne measurements of tropospheric nitrogen dioxide in the Po basin, J. Geophys. Res.-Atmos., 109, D15307, doi:10.1029/2004JD004547, 2004.

Platt, U.: Differential Optical Absorption Spectroscopy (DOAS), in: vol. 127 of Air Monitoring by Spectroscopic Technique, Chemical Analysis Series, 27, John Wiley & Sons, Inc., Hoboken, N.J., USA, 1994.

Platt, U. and Stutz, J.: Differential Optical Absorption Spectroscopy: Principles and Applications, Springer, Berlin, Heidelberg, Germany, 2008.

Salam, M. T., Islam, T., and Gilliland, F. D.: Recent evidence for adverse effects of residential proximity to traffic sources on asthma, Current Opin. Pulmon. Med., 14, 3–8, 2008.

Schaub, D., Boersma, K. F., Kaiser, J. W., Weiss, A. K., Folini, D., Eskes, H. J., and Buchmann, B.: Comparison of GOME tropospheric NO_2 columns with NO_2 profiles deduced from ground-based in situ measurements, Atmos. Chem. Phys., 6, 3211–3229, doi:10.5194/acp-6-3211-2006, 2006.

Seinfeld, J. H. and Pandis, S. N.: Atmospheric Chemistry and Physics: From Air Pollution to Climate Change, 2nd Edn., John Wiley & Sons Inc., Hoboken, N.J., 2006.

Shaiganfar, R., Beirle, S., Sharma, M., Chauhan, A., Singh, R. P., and Wagner, T.: Estimation of NO_x emissions from Delhi using Car MAX-DOAS observations and comparison with OMI satellite data, Atmos. Chem. Phys., 11, 10871–10887, doi:10.5194/acp-11-10871-2011, 2011.

Simpson, D., Benedictow, A., Berge, H., Bergström, R., Emberson, L. D., Fagerli, H., Flechard, C. R., Hayman, G. D., Gauss, M., Jonson, J. E., Jenkin, M. E., Nyíri, A., Richter, C., Semeena, V. S., Tsyro, S., Tuovinen, J.-P., Valdebenito, Á., and Wind, P.: The EMEP MSC-W chemical transport model – technical description, Atmos. Chem. Phys., 12, 7825–7865, doi:10.5194/acp-12-7825-2012, 2012.

Sinreich, R., Friess, U., Wagner, T., and Platt, U.: Multi axis differential optical absorption spectroscopy (MAX-DOAS) of gas and aerosol distributions, Faraday Discuss., 130, 153–164, 2005.

Stammes, P.: Spectral radiance modelling in the UV-visible range, in: IRS 2000, Current problems in atmospheric radiation, edited by: Smith, W. and Timofeyev, Y. A., Deepak Publishing, Hampton, VA, 385–388, 2001.

Steinbacher, M., Zellweger, C., Schwarzenbach, B., Bugmann, S., Buchmann, B., Ordóñez, C., Prevot, A. S. H., and Hueglin, C.: Nitrogen oxide measurements at rural sites in Switzerland: bias of conventional measurement techniques, J. Geophys. Res.-Atmos., 112, D11307, doi:10.1029/2006JD007971, 2007.

Toronto Transportation Services: Traffic Safety Unit 2010-9-30: Average Weekday, 24 Hour Traffic Volume, Most Recent Counts from 2005–2009, http://www.toronto.ca/transportation/publications/brochures/24hourvolumemap.pdf (last access: 18 October 2013), 2010.

Valari, M., Martinelli, L., Chatignoux, E., Crooks, J., and Garcia, V.: Time scale effects in acute association between air pollution and mortality, Geophys. Res. Lett., 38, L10806, doi:10.1029/2011GL046872, 2011.

Vandaele, A. C., Hermans, C., Simon, P. C., Van Roozendael, M., Guilmot, J. M., Carleer, M., and Colin, R.: Fourier Transform Measurement of NO_2 Absorption Cross-sections in the Visible Range at Room Temperature, J. Atmos. Chem., 25, 289–305, 1996.

Vandaele, A. C., Hermans, C., Simon, P. C., Carleer, M., Colin, R., Fally, S., Mérienne, M. F., Jenouvrier, A., and Coquart, B.: Measurements of the NO_2 absorption cross-section from 42 000 cm^{-1} to 10 000 cm^{-1} (238–1000 nm) at 220 K and 294 K, J. Quant. Spectrosc. Ra., 59, 171–184, doi.10.1016/S0022-4073(97)00168-4, 1998.

Villena, G., Kleffmann, J., Kurtenbach, R., Wiesen, P., Lissi, E., Rubio, M. A., Croxatto, G., and Rappenglück, B.: Vertical gradients of HONO, NO_x and O_3 in Santiago de Chile, Atmos. Environ., 45, 3867–3873, doi:10.1016/j.atmosenv.2011.01.073, 2011.

Vlemmix, T., Piters, A. J. M., Stammes, P., Wang, P., and Levelt, P. F.: Retrieval of tropospheric NO_2 using the MAX-DOAS method combined with relative intensity measurements for aerosol correction, Atmos. Meas. Tech., 3, 1287–1305, doi:10.5194/amt-3-1287-2010, 2010.

Vlemmix, T., Piters, A. J. M., Berkhout, A. J. C., Gast, L. F. L., Wang, P., and Levelt, P. F.: Ability of the MAX-DOAS method to derive profile information for NO_2: can the boundary layer and free troposphere be separated?, Atmos. Meas. Tech., 4, 2659–2684, doi:10.5194/amt-4-2659-2011, 2011.

Wagner, T., Dix, B., v. Friedeburg, C., Frieß, U., Sanghavi, S., Sinreich, R., and Platt, U.: MAX-DOAS O_4 measurements: A new technique to derive information on atmospheric aerosols – Principles and information content, J. Geophys. Res.-Atmos., 109, D22205, doi:10.1029/2004JD004904, 2004.

Wagner, T., Ibrahim, O., Shaiganfar, R., and Platt, U.: Mobile MAX-DOAS observations of tropospheric trace gases, Atmos. Meas. Tech., 3, 129–140, doi:10.5194/amt-3-129-2010, 2010.

Wagner, T., Beirle, S., Brauers, T., Deutschmann, T., Frieß, U., Hak, C., Halla, J. D., Heue, K. P., Junkermann, W., Li, X., Platt, U., and Pundt-Gruber, I.: Inversion of tropospheric profiles of aerosol extinction and HCHO and NO_2 mixing ratios from MAX-DOAS observations in Milano during the summer of 2003 and comparison with independent data sets, Atmos. Meas. Tech., 4, 2685–2715, doi:10.5194/amt-4-2685-2011, 2011.

Wang, S., Xing, J., Chatani, S., Hao, J., Klimont, Z., Cofala, J., and Amann, M.: Verification of anthropogenic emissions of China by satellite and ground observations, Atmos. Environ., 45, 6347–6358, doi:10.1016/j.atmosenv.2011.08.054, 2011.

Wang, Y. J., DenBleyker, A., McDonald-Buller, E., Allen, D., and Zhang, M. K.: Modeling the chemical evolution of nitrogen oxides near roadways, Atmos. Environ., 45, 43–52, doi:10.1016/j.atmosenv.2010.09.050, 2011.

Wang, X., Mallet, Vi., Berroir, J.-P., and Herlin, I.: Assimilation of OMI NO_2 retrievals into a regional chemistry-transport model for improving air quality forecasts over Europe, Atmos. Environ., 45, 485–492, doi:10.1016/j.atmosenv.2010.09.028, 2011.

Wittrock, F., Oetjen, H., Richter, A., Fietkau, S., Medeke, T., Rozanov, A., and Burrows, J. P.: MAX-DOAS measurements of atmospheric trace gases in Ny-Ålesund – Radiative transfer studies and their application, Atmos. Chem. Phys., 4, 955–966, doi:10.5194/acp-4-955-2004, 2004.